

Oxygen and nutrient trends in the Tropical Oceans

Lothar Stramma and Sunke Schmidtke

GEOMAR Helmholtz Centre for Ocean Research Kiel, Düsternbrooker Weg 20, 24105 Kiel, Germany

Correspondence to: Lothar Stramma (lstramma@geomar.de)

Abstract. An oxygen decrease of the intermediate-depth low-oxygen zones (300 to 700 m) is seen in time series for selected tropical areas for the period 1960 to 2008, in the eastern tropical Atlantic, the equatorial Pacific and the eastern tropical Indian Ocean. These nearly five decade-long time series were extended to 68 years by including rare historic data starting in 1950 and more recent data. For the extended time series between 1950 and 2018 the deoxygenation trend for the layer 300 to 700 m is similar to the deoxygenation trend seen in the shorter time series. Additionally, temperature, salinity and nutrient time series in the upper ocean layer (50 to 300 m) of these areas were investigated since this layer provides critical pelagic habitat for biological communities. Generally, oxygen is decreasing in the 50 to 300 m layer except for an area in the eastern tropical South Atlantic. Nutrients also showed long-term trends in the 50 to 300 m layer in all ocean basins and indicate overlying variability related to climate modes. Nitrate increased in all areas. Phosphate also increased in the Atlantic and Indian Ocean areas, while it decreased in the two areas of the equatorial Pacific Ocean. Silicate decreased in the Atlantic and Pacific areas but increased in the eastern Indian Ocean. Hence oxygen and nutrients show trends in the tropical oceans, though nutrients trends are more variable between ocean areas than the oxygen trends, therefore we conclude that those trends are more dependent on local drivers in addition to a global trend. Different positive and negative trends in temperature, salinity, oxygen and nutrients indicate that oxygen and nutrient trends cannot be completely explained by local warming.

1 Introduction

Temperature, oxygen and nutrient changes in the ocean have various impacts on the ecosystem. These impacts span from habitat compression in the open ocean (Stramma et. al., 2012) and affect all marine organisms through multiple direct and indirect mechanisms (Gilly et al., 2013) to affect the ecophysiology of marine water-breathing organisms with regard to distribution, phenology and productivity (Cheung et al., 2013). Despite its far-reaching consequences for humanity, the focus on climate change impacts on the ocean lags behind the concern for impacts on the atmosphere and land (Allison and Bassett, 2015). An oceanic increase in stratification, thus reduction in ventilation as well as decrease of oceanic dissolved oxygen are two of the less obvious but important expected indirect consequences of climate change on the ocean (Shepherd et al., 2017). Warming leads to lighter water in the surface layer and increased stratification reducing the mixing and deep ventilation of oxygen-rich surface water to the subsurface layers. Increasing ocean stratification over the last half century of about 5% is observed in the upper 200 m (Li et al. 2020). The subsequent previously observed deoxygenation (e.g. Stramma et al, 2008,

31 Schmidtko et al 2017) of the open ocean is one of the major manifestations of global change. This temperature oxygen relation
32 can also be seen for the 0-1000 m layer of the global ocean, as the oxygen inventory is negatively correlated with the ocean
33 heat content ($r=-0.86$; 0-1000 m) (Ito et al., 2017). Oxygen-poor waters often referred to as oxygen minimum zones (OMZ)
34 occupy large volumes of the intermediate-depth eastern tropical oceans. In an investigation of six selected areas for the 300 to
35 700 m layer in the tropical oceans for the time period 1960 to 2008 Stramma et al. (2008) observed declining oxygen
36 concentrations of -0.09 to $-0.34 \mu\text{mol kg}^{-1} \text{ year}^{-1}$ and a vertical expansion of the intermediate depth low oxygen zone. Such a
37 vertical expansion of the OMZ that is entered and passed by diel vertical migrators and sinking particles could have widespread
38 effects on species distribution, the biological pump and benthic-pelagic coupling (Wishner et al., 2013). The areas of the world
39 ocean investigated for oxygen changes can be extended and in a quantitative assessment of the entire world ocean oxygen
40 inventory by analysing dissolved oxygen and supporting data for the complete oceanic water column over the past 50 years
41 since 1960. Schmidtko et al. (2017) reported that the global oceanic oxygen content of 227.4 ± 1.1 petamoles (10^{15}mol) has
42 decreased by more than two percent (4.8 ± 2.1 petamoles). However, these oxygen changes vary by region with some areas
43 showing increasing oxygen values on time scales related to climate modes.

44 The nutrient distribution is in addition to oxygen a key parameter controlling the marine ecosystems. However, very little is
45 known about long term nutrient changes in the ocean. The transformation of carbon and nutrients into organic carbon, its
46 sinking, advection and subduction into the in the deep ocean, and its decomposition at depth, is known as the biological carbon
47 pump. As a consequence, nutrients are consumed and thus lower in the surface ocean and released and thus higher in the deep
48 ocean. The oceanic distribution of nutrients and patterns of biological production are controlled by the interplay of
49 biogeochemical and physical processes, and external sources (Williams and Follows, 2003). In the upper 500 to 1000 m of the
50 tropical oceans the nutrient concentration is higher than in the subtropics and is decreasing westwards (Levitus et al., 1993).
51 In the subarctic North Pacific surface nutrient concentration decreased during 1975 to 2005, and is strongly correlated with a
52 multidecadal increasing trend of sea surface temperature (SST) (Ono et al., 2008). Below the surface, however, oxygen
53 decreased and nutrients increased in the subarctic Pacific pycnocline from the mid-1980s to around 2010 (Whitney et al.,
54 2013). Nutrients would be expected to vary inversely with oxygen, if the dominant process was the remineralization of marine
55 detritus (Whitney et al., 2013). In a recent study the trends of nutrients in the open Pacific Ocean were investigated (Stramma
56 et al., 2020) and in the open Pacific Ocean nutrient trends were observed and seemed to be related to oxygen trends. The supply
57 of nutrients to the sunlit surface layer of the ocean has traditionally been attributed solely to vertical processes. However,
58 horizontal advection may also be important in establishing the availability of nutrients in some regions. Palter et al. (2005)
59 showed that the production and advection of North Atlantic Subtropical Mode Water introduces spatial and temporal variability
60 in the subsurface nutrient reservoir beneath the North Atlantic subtropical gyre. By means of a coupled ecosystem circulation
61 model Oschlies (2001) described for the North Atlantic that the long-term change in the North Atlantic Oscillation (NAO; e.g.
62 Hurrell and Deser, 2010) between the 1960s and 1990s may have induced significant regional changes in the upper ocean's
63 nutrient supply. These include a decrease of nitrate supply to the surface waters of by about 30% near Bermuda and in mid
64 latitudes, and a simultaneous 60% increased nitrate flux in the upwelling region off West Africa. On the other side of the globe

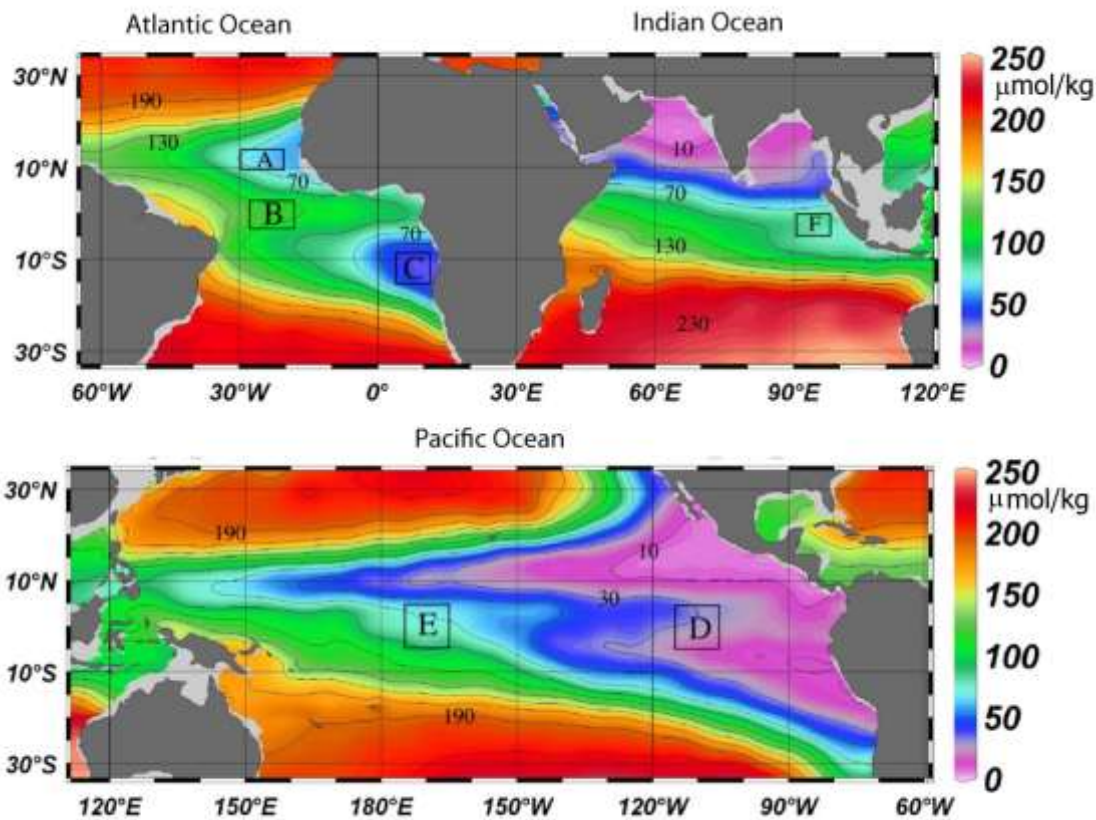
65 the Indonesian throughflow (ITF) is a chokepoint in the upper ocean thermohaline circulation, carrying Pacific waters through
66 the strongly mixed Indonesian Seas and into the Indian Ocean (Ayers et al., 2014). Ayers et al. (2014) determined the depth-
67 and time-resolved nitrate, phosphate, and silicate fluxes at the three main exit passages of the ITF: Lombok Strait, Ombai
68 Strait, and Timor Passage. Nutrient flux as well as its variability with depth and time differed greatly between the passages.
69 They estimated the effective flux of nutrients into the Indian Ocean and found that the majority of ITF nutrient supply to the
70 Indian Ocean is to thermocline waters, where it is likely to support new production and significantly impact Indian Ocean
71 biogeochemical cycling.

72 Here we investigate the extent of changes in oxygen, temperature and salinity trends for the six tropical areas with longer time
73 series compared to the previously about one third shorter timeseries. Additionally, trends in the biologically active near
74 surface layer 50 to 300 m are investigated. As the upper ocean provides critical pelagic habitat for biological communities,
75 nutrient time series of the six tropical areas since 1950 are investigated at 50 to 300 m depth, as nutrient changes in combination
76 with hydrographic changes will influence the biological productivity of the ocean (Sigman and Hain, 2012). The upper
77 boundary of 50 m was chosen to reduce the influence of the seasonal cycle in the upper 50 m although the seasonal cycle in
78 the tropics is weaker than in most subtropical and subpolar regions (Louanchi and Najjar, 2000). As there are indications that
79 climate modes and the El Niño-Southern Oscillation (ENSO) events have an influence on the trends, we check whether these
80 signals are apparent in the data in the near surface layer.

81 **2 Data and methods**

82 Stramma et al. (2008) investigated the temperature and oxygen trends for the period 1960 to 2008 in the 300 to 700 m layer of
83 six tropical ocean areas. There were three areas in the tropical Atlantic (A: 10°–14°N, 20°–30°W; B: 3°S–3°N, 18°–28°W; C:
84 14°S–8°S, 4°–12°E), two areas in the eastern and central tropical Pacific (D: 5°S–5°N, 105°–115°W; E: 5°S–5°N, 165°–175°W)
85 and one in the eastern Indian Ocean (F: 5°S–0°N, 90°–98°E) (Figure 1). Here these time series were extended with more recent
86 data as well as back in time to 1950 for the regions with available data (Table 1 and Figure 2).

87



88

89 **Figure 1:** Climatological mean dissolved oxygen concentration ($\mu\text{mol kg}^{-1}$ shown in color) at 400 m depth contoured at 20
 90 $\mu\text{mol kg}^{-1}$ intervals from 10 to 230 $\mu\text{mol kg}^{-1}$ (black lines). Analysed areas A to F (Table 1) are enclosed by black boxes
 91 (Stramma et al., 2008).

92

93 Despite long-term trends in ocean oxygen also climate signal related influence on the trends was observed in recent years.
 94 More recently also long-term trends and climate signal related influence was observed for nutrients. The areas D and E were
 95 also used for the layer 50 to 300 m for oxygen changes in Stramma et al. (2020), but not for nutrient trends due to the low
 96 amount of available nutrients data. However, here we list also the nutrients trends for these two areas, despite the fact that the
 97 low amount of data does not make these calculations statistically significant (Table 2).

98 The main hydrographic data set is similar to the one used and described in Schmidtko et al. (2017), relying on Hydrobase 2
 99 and World Ocean Database bottle data for nutrient data. Quality control and handling is described in Schmidtko et al. (2017)
 100 for oxygen and is used here similarly for nutrients. Summarizing the most important steps, only profiles with plausible values
 101 were used, profiles with linear or constant values over depths removed, duplicates detected within 5km and 25h and the one
 102 with best vertical resolution used, database control flags were observed and a minimum divergence of values required. The

103 only divergence to the described procedure is that bottle data with missing temperature and/or salinity were assigned the
104 temporal and spatial interpolated temperature and salinity derived from MIMOC (Schmidtko et al., 2013). This was done to
105 ensure all data were in $\mu\text{mol kg}^{-1}$ and not requiring the discarding of already sparse data due to missing water density
106 (temperature and salinity) values. This enables us to use data provided in the data bases in mol l^{-1} or ml l^{-1} which otherwise
107 could not be used.

108 As a main focus of the computations is the comparison with the results of Stramma et al. (2008), we applied similar methods
109 for a direct comparison. All data from bottle as well as CTD measurements within a selected area sampled within one year
110 were combined independent of the season and location and then used for the trend computation. As in Stramma et al. (2008)
111 the amount of data was too small to further distinguish for season and location within the area. Profiling float data were not
112 used as oxygen measurements on our floats showed drifts in time probably due to biological activity on the sensors which
113 could lead to biased trends. Earlier measurements from bottle data had less accurate depth measurements as well as fewer
114 vertical measurements compared to years with CTD profiles within the selected depth layers. This can add some uncertainty
115 to earlier measurements, though no systematic bias towards increasing or decreasing oxygen trends. For years with CTD
116 measurements on 1 dbar steps the uncertainties between years will be significant less than those years with only bottle data.
117 Mean parameter values for each layer was computed from the annual mean values in the selected depth layer. The standard
118 deviation of the parameter values depends both on the variability of the annual mean parameter value as well as the strength
119 of the trend during the measurement period.

120 In the Atlantic the hydrographic and nutrient data were extended with some *RV Meteor*, *RV Merian* and *RV Poseidon* cruises.
121 For the area A data from Meteor cruises M68/2 (2006), M83/1 (2008), M97 (2010), M119 (2015) and M145 (2018) and Merian
122 MSM10/1 (2008) were added. For area B Meteor cruises M106 (2014), M130 (2016) and M145 (2018) were added. For area
123 C cruise data from Poseidon P250 (1999), Merian MSM07 (2008), Meteor M120 (2015), Meteor M131 (2016) and Meteor
124 M148 (2018) were included.

125 The Pacific the region at 5°N – 5°S , 165 – 175°W (area E) which had data until 2009 was supplemented with data from a *RV*
126 *Investigator* cruise at 170°W from June 2016. The region 5°N – 5°S , 105 – 110°W (area D), which had data up to 2008, was
127 supplemented with data from a *RV Ron Brown* cruise at 110°W in December 2016.

128 Climate indices considered include the NAO, the AMO, the PDO, ENSO, as well as the Indian Ocean Dipole Mode (IOD).
129 The NAO is an extratropical climate signal of the North Atlantic. As our areas are tropical regions the three Atlantic areas
130 were investigated relative to the Atlantic Multidecadal Oscillation (AMO) index (Montes et al., 2016) before and after 1995.
131 The AMO was high before 1963, low until 1995 and high since 1995. In the Pacific the central equatorial area at 5°N – 5°S ,
132 165° – 175°W (area E in Stramma et al., 2008) which had hydrodata until 2009, was supplemented with data from a *RV*
133 *Investigator* cruise at 170°W from June 2016. The eastern equatorial area 5°N – 5°S , 105° – 115°W (area D in Stramma et al.
134 2008), which had hydrodata until 2008, was supplemented with data from a *RV Ron Brown* cruise at 110°W in December
135 2016. The data were investigated in relation to the Pacific Decadal Oscillation (PDO; e.g. Deser et al., 2010) before and after
136 1977. The PDO was negative from 1944 to 1976, positive from 1977 to 1998, variable from 1998 to 2013 and positive after

137 2013. In the Indian Ocean the available data covered the area F only after 1960 but until 2016. The area F (0° to 5°S, 90° to
138 98°E) is shown in relation to the IOD (Saji et al., 1999), which slightly increased after 1990.

139 Linear trends and their 95% confidence interval were computed by using annual averages (all measurements within one year
140 were attributed to that year) of the profiles linearly interpolated to standard vertical depth levels. A computation routine was
141 used to derive the effective number of degrees of freedom for the computation of the confidence interval. The data used for
142 the oxygen time series were interpolated to 5 dbar steps with an objective mapping scheme (Bretherton et al., 1976) with
143 Gaussian weighting. In the 50 to 300 m layer and the 300 to 700 m a temporal half folding range of 0.5 year and a vertical half
144 folding range of 50 m with maximum ranges of 1 year and 100 m respectively were applied. The covariance matrix was
145 computed from the closest 100 local data points and 50 random data points within the maximum range, for the diagonal of the
146 covariance matrix a signal to noise ratio of 0.7 was set (see Schmidtko et al. 2013, for details). A more improved mapping
147 scheme was used compared to the one used in Stramma et al. (2008) where larger temporal ranges were used (1-year half
148 folding and a maximum temporal range of 2 years).

149 Nutrients nitrite (NO₂⁻), nitrate (NO₃⁻), phosphate (PO₄³⁻) and silicic acid (Si(OH)₄ referred to as silicate hereafter) on the recent
150 cruises were measured on-board with a QuAAtro auto-analyzer (Seal Analytical). For recent autoanalyzer measurements
151 precisions are 0.01 μmol kg⁻¹ for phosphate, 0.1 μmol kg⁻¹ for nitrate, and 0.5 μmol kg⁻¹ for silicate and 0.02 mL L⁻¹ (~ 0.9
152 μmol kg⁻¹) for oxygen from Winkler titration (Bograd et al., 2015). For older uncorrected nutrient data, offsets are estimated
153 to be 3.5% for nitrate, 6.2% for silicate and 5.1% for phosphate (Tanhua et al., 2010). One problem with nutrient data is that
154 certified reference material (CRM) was applied to some measurements while for other measurements only a bias was applied.
155 Inter-cruise offsets were investigated for the deep ocean between WOCE (World Ocean Circulation Experiment) and non-
156 WOCE cruises and resulted in root-mean-square inter-cruise offsets before adjustment of 0.003 g kg⁻¹ for salinity, 2.498 μmol
157 kg⁻¹ for oxygen, 2.4 μmol kg⁻¹ for silicate, 0.55 μmol kg⁻¹ for nitrate and 0.045 μmol kg⁻¹ for phosphate (Gouretski and Jancke,
158 2001), while Johnson et al. (2001) presented initial standard deviations of crossover differences of WOCE cruises of 0.0028
159 for salinity, 2.1% for oxygen, 2.8% for nitrate, 1.6% for phosphate and 2.1% for silicic acid. Hence a slight bias based on the
160 measurements applied could be included in the measurements.

161 The ENSO cycle of alternating warm El Niño and cold La Niña events is the climate system's dominant year-to year signal.
162 ENSO originates in the tropical Pacific through interaction between the ocean and the atmosphere, but its environmental and
163 socioeconomic impacts are felt worldwide (McPhaden et al., 2006). Three month running mean SST anomalies (ERSST.v5
164 SST anomalies) in the Niño 3.4 region (equatorial Pacific: 5°N to 5°S, 120°W to 170°W) of at least +0.5°C and lasting for at
165 least 5 consecutive three months periods are defined as El Niño events and 5 consecutive three months periods of at least -
166 0.5°C are defined as La Niña events (http://origin.cpc.ncep.noaa.gov/products/analysis_monitoring/ensostuff/ONI_v5.php). In
167 case of measurements in ENSO years in figures 3, 4 and 5 the very strong El Niño events of 1983, 1998 and 2015 and the
168 strong El Niño events 1957, 1965, 1972, 1987 and 1991 are marked by red circles and the strong La Niña events 1974, 1976,
169 1989, 1999, 2000, 2007 and 2010 are marked by blue squares in these years. A shoaling thermocline, such as occurs in the
170 eastern Pacific during La Niña or cool (negative) PDO state, enhances nutrient supply and organic matter export in the eastern

171 Pacific while simultaneously increasing the fraction of that organic matter that is respired in the low-oxygen water of the
 172 uplifted thermocline. The opposite occurs during El Niño or a warm (positive) PDO state; a deeper thermocline reduces both
 173 export and respiration in low-oxygen water in the eastern Pacific, allowing the hypoxic water volume to shrink (Deutsch et al.,
 174 2011; Fig. S7). ENSO also has some influence on the tropical Atlantic and Indian Oceans. The equatorial Atlantic oscillation
 175 is influenced by the Pacific ENSO with the equatorial Atlantic sea surface temperature lagging by about six months (Latif and
 176 Grötzner, 2000). In the Indian Ocean a recent weakening of the coupling between the ENSO and the IOD mode after the 2000s
 177 and 2010s compared to the previous two decades (1980s and 1990s) (Ham et al., 2017).

178
 179

180 **3 Trends in temperature, salinity, oxygen and nutrients**

181 **3.1 Trends in the 300 to 700 m depth layer**

182 Nutrient data are sparse in the deeper part of the ocean and are less important than the near surface layer for the marine
 183 ecosystems and therefore are not presented here for the 300 to 700 m depth layer. Oxygen trends for the period 1960 to 2008
 184 for the 300 to 700 m layer of the six areas investigated (Stramma et al., 2008) for the tropical oceans were all negative in the
 185 range -0.09 to -0.34 $\mu\text{mol kg}^{-1} \text{ year}^{-1}$ (Table 1). For the extended time period between 1950 and 2018 the oxygen trends were
 186 in the same order of magnitude for the areas A to F in the range -0.11 to -0.27 $\mu\text{mol kg}^{-1} \text{ year}^{-1}$ (Table 1). The 1950 to 2018
 187 temperature trends were positive in the three Atlantic areas and the eastern tropical Pacific, but negative in the central Pacific
 188 and Indian Ocean areas (Table 1). In the eastern tropical Pacific (area D) and the eastern Indian Ocean (area F) there was even
 189 a reversed trend in temperature compared to the shorter time period between 1960 and 2008, although all temperature trends
 190 are not within the 95% confidence interval difference from 0. The salinity of the 300 to 700 m layer increased for the Atlantic
 191 and Indian Ocean areas and decreased in the two Pacific areas (Table 1).

192
 193

194 **Table 1.** Linear trends (300 to 700 m) of temperature in $^{\circ}\text{C yr}^{-1}$, oxygen in $\mu\text{mol kg}^{-1} \text{ yr}^{-1}$ and salinity yr^{-1} with 95% confidence
 195 intervals (p-values) where data are available for the entire period listed. Trends whose 95% confidence interval includes zero
 196 are shown in *italics*. Trends computed in Stramma et al. (2008) are shown for comparison.

197	Parameter	trend	time period	depth layer	(Stramma et al., 2008)
198	Area A	10°N-14°N, 20°W-30°W			
199	Temperature	+0.009 ± 0.005	1952-2018	300-700 m	+0.009 ± 0.008 1960-2006 300-700 m
200	Oxygen	-0.27 ± 0.12	1952-2018	300-700 m	-0.34 ± 0.13 1960-2006 300-700 m
201	Salinity	+0.0012 ± 0.0009	1952-2018	300-700 m	

202

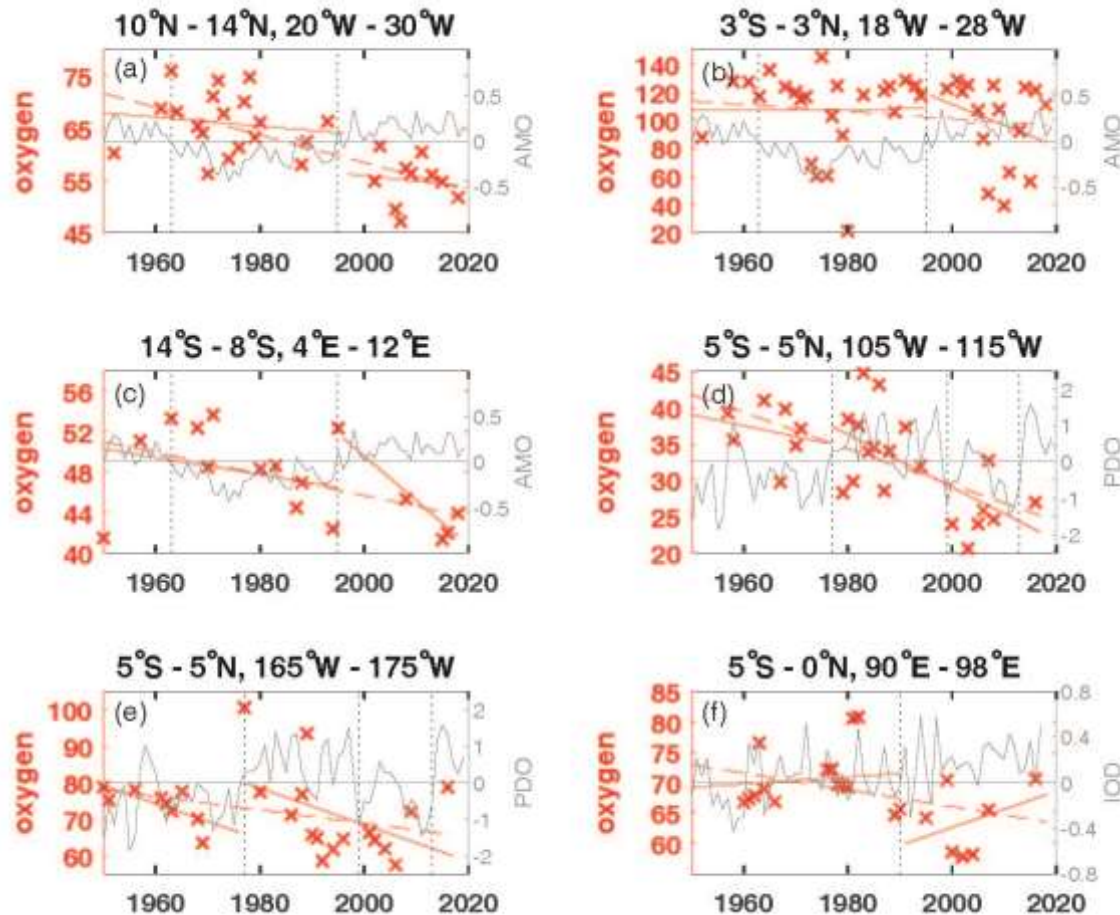
203	Area B	3°S-3°N, 18°W-28°W		
204	Temperature	+0.005 ± 0.004	1952-2018	300-700 m
				+0.005 ± 0.008 1960-2006 300-700 m
205	Oxygen	-0.25 ± 0.65	1952-2018	300-700 m
				-0.19 ± 0.12 1960-2006 300-700 m
206	Salinity	+0.0001 ± 0.0005	1952-2018	300-700 m
207				
208	Area C	14°S-8°S, 4°E-12°E		
209	Temperature	+0.006 ± 0.004	1950-2018	300-700 m
				+0.002 ± 0.011 1961-2008 300-700 m
210	Oxygen	-0.11 ± 0.100	1950-2018	300-700 m
				-0.17 ± 0.11 1961-2008 300-700 m
211	Salinity	+0.0005 ± 0.0009	1950-2018	300-700 m
212				
213	Area D	5°S-5°N, 105°W-115°W		
214	Temperature	+0.003 ± 0.004	1955-2016	300-700 m
				-0.001 ± 0.009 1962-2006 300-700 m
215	Oxygen	-0.24 ± 0.15	1957-2016	300-700 m
				-0.13 ± 0.32 1962-2006 300-700 m
216	Salinity	-0.0001 ± 0.009	1950-2016	300 -700 m
217				
218	Area E	5°S-5°N, 165°W-175°W		
219	Temperature	-0.001 ± 0.011	1950-2016	300-700 m
				-0.010 ± 0.008 1961-2006 300-700 m
220	Oxygen	-0.18 ± 0.25	1950-2016	300-700 m
				-0.19 ± 0.20 1961-2006 300-700 m
221	Salinity	-0.0003 ± 0.0009	1950-2016	300-700 m
222				
223	Area F	5°S-0°N, 90°E-98°E		
224	Temperature	-0.004 ± 0.010	1960-2016	300-700 m
				+0.005 ± 0.007 1960-2007 300-700 m
225	Oxygen	-0.13 ± 0.17	1960-2016	300-700 m
				-0.09 ± 0.21 1960-2007 300-700 m
226	Salinity	+0.0001 ± 0.0010	1960-2016	300-700 m

229

230

231 For the area A (10°-14°N, 20°-30°W) the oxygen trend for 300 to 700 m for the period 1952 to 2018 (Figure 2a) was weaker
232 (-0.27 ± 0.12 μmol kg⁻¹ yr⁻¹) than for the period 1960 to 2006 (-0.34 ± 0.13 μmol kg⁻¹ yr⁻¹). In the western subtropical and
233 tropical Atlantic oxygen measurements from time series stations as well as shipboard measurements showed a significant
234 relationship with the wintertime AMO index (Montes et al., 2016). During negative wintertime AMO years trade winds are
235 typically stronger and these conditions stimulate the formation and ventilation of Subtropical Underwater (Montes et al., 2016)

236 with higher oxygen content. Even in the 300 to 700 m layer of Area A (Figure 2a) as well as the 50 to 300 m layer (Figure 3a)
 237 the oxygen content is higher during the negative AMO period and lower during the positive AMO phase. For a section along
 238 23°W between 6°–14°N from 2006 to 2015 crossing area A an oxygen decrease in the 200 to 400 m layer and an increase in
 239 the 400 to 1000 m layer was described (Hahn et al., 2017) which can't be confirmed in area A due to the different geographical
 240 and temporal boundaries and the variable annual mean oxygen values after 2006 in area A.
 241 The 1952 to 2018 oxygen trend in the equatorial Atlantic (area B) shows a large 95% confidence interval, different to the
 242 shorter time period 1960 to 2006 (Table 1). The larger confidence interval is caused by a low oxygen concentration in 1952
 243 and large variability after 2006 (Figure 2b). The equatorial Atlantic in the depth range 500 to 2000 m is influenced by Equatorial
 244 Deep Jets with periodically reversing flow direction influencing the transport of oxygen (Bastin et al., 2020) which might be
 245 one reason of the large oxygen variability. During the negative AMO the oxygen trend was slightly positive (-0.034 ± 1.39
 246 $\mu\text{mol kg}^{-1} \text{yr}^{-1}$) but negative after 1995 (Figure 2b).
 247
 248



249

250

251 **Figure 2:** Annual mean oxygen concentration for years available (x) used to calculate trends for the layer 300 to 700 m in
252 $\mu\text{mol kg}^{-1}$ plotted for the available years in the time period 1950 to 2018 (dashed red line) and for the positive and negative
253 periods of the AMO in the Atlantic (a-c), the PDO in the Pacific (d,e) and the IOD in the Indian Ocean (f) as solid red lines.
254 The AMO, PDO and IOD are shown as grey lines. The change of AMO status in 1963 and 1995, the change of the PDO phase
255 in 1977, 1999 and 2013 and the IOD in 1990 are marked by dotted vertical lines. The scale of the y-axis changes according to
256 the oxygen concentration of each area.

257

258

259 The area C in the eastern tropical South Atlantic shows similar positive trends in temperature and salinity (Table 1) as in the
260 two other Atlantic areas investigated. Area C is located in the region with the lowest oxygen content in the Atlantic Ocean
261 (Figure 1). Due to the already low oxygen concentration in this region the decrease in oxygen is weaker than in the two other
262 Atlantic Ocean areas in the period 1950 to 2018, similar to the weaker decrease in area C for the shorter time period 1961 to
263 2008 (Table 1). Higher oxygen concentrations were also seen in the few oxygen profiles in area C during the negative AMO
264 and lower oxygen concentrations were measured after the year 2000 (Figure 2c).

265 In the equatorial Pacific the two areas show a clear long-term oxygen decrease in the 300 to 700 m layer, but no clear changes
266 related to the PDO phases before and after 1977 (Figure 2d,e). However, the PDO-index after 1977 was mainly positive until
267 1999 and mainly negative between 1999 and 2013. In case these time periods are looked at separately the oxygen concentration
268 was higher during the period 1977 to 1990 and lower during 1999 to 2010 as expected for the PDO influence (e.g. Deutsch et
269 al. 2011).

270 In the eastern Indian Ocean, the 300 to 700 m oxygen concentration was lower for the slightly positive IOD phase after 1990
271 leading to a long-term oxygen concentration decrease in area F although the trends for the shorter periods prior to 1990 and
272 after 1990 showed a positive oxygen trend (Figure 2f), which are caused by high oxygen concentrations near the end of both
273 measurement periods. The temperature in this area decreased and salinity showed barely any change (Table 1), hence the
274 oxygen decrease is not coupled to temperature or hydrographic water mass changes.

275

276 **3.2 Trends in the 50 to 300 m layer**

277 The trend computations for the layer 50 to 300 m for temperature, salinity, oxygen and nutrients (Table 2) show different
278 trends for the selected areas in the three tropical oceans. In the near surface layer 50 to 300 m the long-term oxygen trends
279 were negative as in the deeper layer 300 to 700 m, except for area C in the eastern tropical South Atlantic (Figure 3c). However,
280 this oxygen trend in area C is not stable due to the large variability in the time period 1960 to 1990. The upper layer of the area
281 C is influenced by the Angola Dome centered at 10°S, 9°E (Mazeika, 1967) which might influence the larger variability near

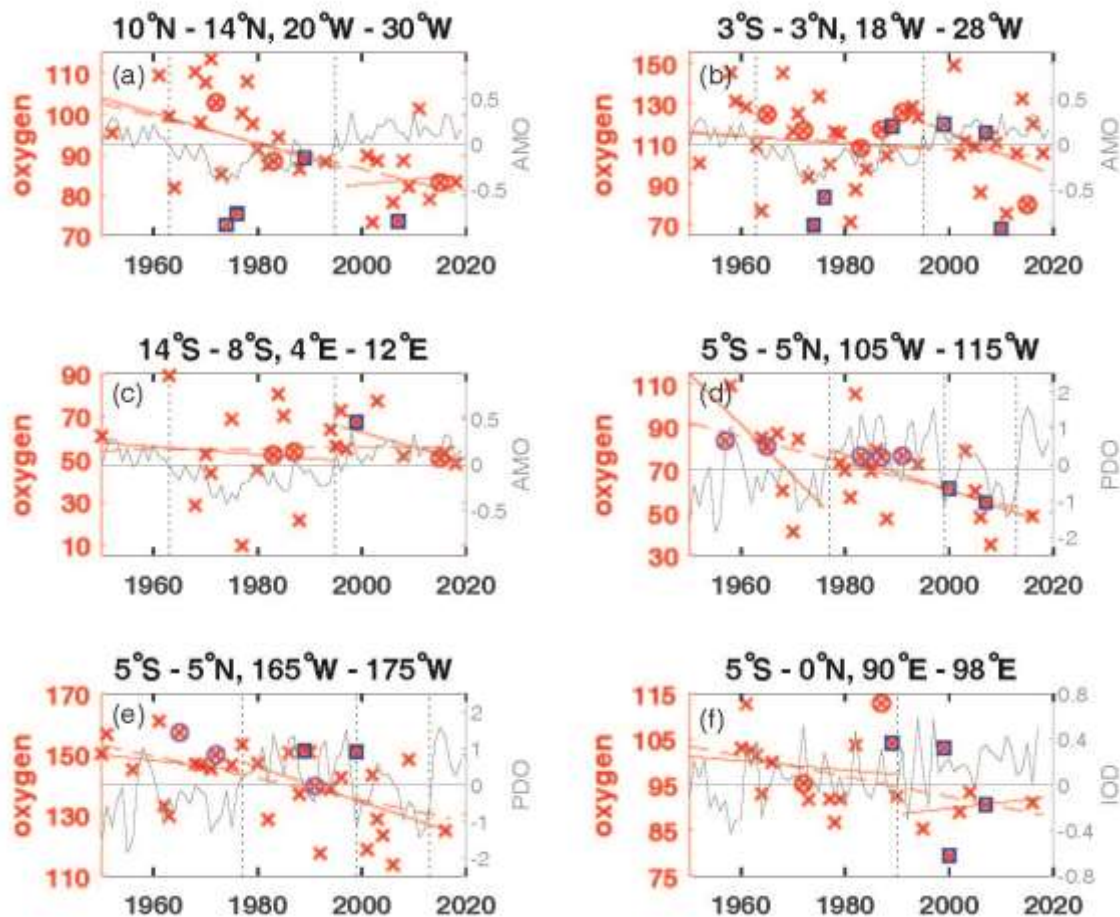
282 the surface. The area C shows the largest mean nitrate, silicate and phosphate concentrations in the Atlantic in the 50 to 300
 283 m layer as well as the 300 to 700 m layer (Table 3) and shows the large nutrient availability in the eastern tropical South
 284 Atlantic. At 250 m and 500 m depth the region of area C was shown with the highest nitrate and phosphate concentrations of
 285 the tropical and subtropical Atlantic Ocean (Levitus et al. 1993). It was observed that in the Pacific Ocean nutrients are related
 286 to oxygen changes and climate variability (Stramma et al., 2020). The ENSO signal was apparent in most cases as in the
 287 tropical Atlantic and Indian Ocean (Nicholson, 1997) hence the oxygen distribution for the layer 50 to 300 m (Figure 3) is
 288 marked for El Niño and La Niña events to check for the possible influence of ENSO in the shallow depth layer. Most of the
 289 nutrient trends are due to sparse data coverage not statistically significant, nevertheless it is insightful to compare the nutrient
 290 trends with the oxygen trends as well as the climate signals.

291
 292 **Table 2.** Linear trends (50-300 m) of temperature in °C yr⁻¹, salinity yr⁻¹ and solutes in μmol kg⁻¹ yr⁻¹ with 95% confidence
 293 intervals (p-values) where data are available for the entire period 1950 to 2018 (left rows) and for the earlier time period (center
 294 rows) and later time period (right rows) separated in 1995 in the Atlantic Ocean (areas A, B, C), in 1977 in the Pacific Ocean
 295 (areas D, E) and 1990 in the Indian Ocean (area F).. Trends whose 95% confidence interval includes zero are shown in *italics*.

296	Parameter	trend	time period	trend	time period	trend	time period
297	Area A	10°N-14°N, 20°W-30°W, 50-300 m					
298	Temperature	<i>+0.007 ± 0.008</i>	1952-2018	<i>+0.004 ± 0.021</i>	1952-1993	<i>-0.001 ± 0.050</i>	2001-2018
299	Salinity	<i>+0.0009 ± 0.0012</i>	1952-2018	<i>+0.27 ± 0.0033</i>	1952-1993	<i>+0.006 ± 0.0083</i>	2001-2018
300	Oxygen	<i>-0.329 ± 0.231</i>	1952-2018	<i>-0.387 ± 0.639</i>	1952-1993	<i>+0.131 ± 1.120</i>	2001-2018
301	Nitrate	<i>+0.038 ± 0.077</i>	1952-2018	<i>+0.112 ± 0.116</i>	1952-1993	<i>-0.022 ± 0.581</i>	2001-2018
302	Silicate	<i>-0.066 ± 0.086</i>	1952-2018	<i>+0.002 ± 0.310</i>	1952-1989	<i>+0.029 ± 0.151</i>	2001-2018
303	Phosphate	<i>+0.001 ± 0.004</i>	1952-2018	<i>-0.002 ± 0.010</i>	1952-1993	<i>-0.024 ± 0.029</i>	2001-2018
304							
305	Area B	3°S-3°N, 18°W-28°W, 50-300 m					
306	Temperature	<i>-0.007 ± 0.012</i>	1952-2018	<i>-0.013 ± 0.028</i>	1952-1995	<i>-0.017 ± 0.042</i>	1997-2018
307	Salinity	<i>+0.0003 ± 0.0011</i>	1952-2018	<i>+0.0001 ± 0.0030</i>	1952-1994	<i>+0.0010 ± 0.0040</i>	1997-2018
308	Oxygen	<i>-0.172 ± 0.421</i>	1952-2018	<i>-0.174 ± 0.874</i>	1952-1994	<i>-1.050 ± 2.010</i>	1999-2018
309	Nitrate	<i>+0.022 ± 0.075</i>	1961-2018	<i>+0.095 ± 0.111</i>	1961-1994	<i>+0.055 ± 0.369</i>	1997-2018
310	Silicate	<i>-0.061 ± 0.041</i>	1961-2018	<i>-0.079 ± 0.107</i>	1961-1994	<i>-0.056 ± 0.144</i>	1999-2018
311	Phosphate	<i>+0.001 ± 0.004</i>	1952-2018	<i>+0.007 ± 0.005</i>	1952-1994	<i>+0.003 ± 0.021</i>	1997-2018
312							
313	Area C	14°S-8°S, 4°E-12°E, 50-300 m					
314	Temperature	<i>+0.006 ± 0.024</i>	1950-2018	<i>+0.018 ± 0.020</i>	1950-1994	<i>+0.04 ± 0.108</i>	1995-2018

315	Salinity	$+0.0008 \pm 0.0020$ 1950-2018	-0.0019 ± 0.0025 1950-1994	$+0.0039 \pm 0.0070$ 1995-2018
316	Oxygen	$+0.028 \pm 0.474$ 1950-2018	-0.183 ± 1.190 1950-1994	-0.675 ± 0.819 1995-2018
317	Nitrate	$+0.051 \pm 0.088$ 1966-2018	$+0.257 \pm 0.220$ 1966-1988	-0.011 ± 0.530 1995-2018
318	Silicate	-0.052 ± 0.077 1968-2018	$+0.020 \pm 0.139$ 1968-1994	-0.161 ± 0.444 1995-2018
319	Phosphate	$+0.002 \pm 0.005$ 1957-2018	$+0.011 \pm 0.008$ 1957-1988	-0.001 ± 0.009 1995-2018
320				
321	Area D	5°S-5°N, 105°W-115°W, 50-300 m		
322	Temperature	$+0.003 \pm 0.019$ 1955-2016	$+0.076 \pm 0.209$ 1955-1975	-0.004 ± 0.094 1979-2016
323	Salinity	-0.0000 ± 0.0018 1955-2016	-0.0017 ± 0.0068 1955-1975	$+0.0001 \pm 0.0022$ 1979-2016
324	Oxygen	-0.643 ± 0.367 1957-2016	-2.390 ± 3.100 1957-1971	-0.825 ± 0.825 1979-2016
325	Nitrate	$+0.033 \pm 0.166$ 1964-2016	$+0.329 \pm 14.90$ 1964-1968	$+0.223 \pm 0.272$ 1983-2016
326	Silicate	-0.001 ± 0.147 1967-2016	$+1.410 \pm 0.921$ 1967-1970	$+0.053 \pm 0.546$ 1983-2016
327	Phosphate	-0.002 ± 0.013 1957-1994	$+0.005 \pm 0.046$ 1957-1971	$+0.035 \pm 0.021$ 1983-1994
328				
329	Area E	5°S-5°N, 165°W-175°W, 50-300 m		
330	Temperature	-0.006 ± 0.020 1950-2016	$+0.026 \pm 0.060$ 1950-1976	-0.010 ± 0.051 1977-2016
331	Salinity	$+0.0005 \pm 0.0026$ 1950-2016	$+0.0005 \pm 0.0100$ 1950-1979	$+0.0000 \pm 0.0058$ 1977-2016
332	Oxygen	-0.361 ± 0.224 1950-2016	-0.192 ± 0.781 1950-1975	-0.570 ± 0.574 1977-2016
333	Nitrate	$+0.054 \pm 0.062$ 1961-2016	$+0.159 \pm 0.366$ 1961-1975	$+0.105 \pm 0.154$ 1977-2016
334	Silicate	-0.046 ± 0.148 1956-2016	$+0.172 \pm \text{NaN}$ 1956-1975	$+0.085 \pm 0.174$ 1977-2016
335	Phosphate	-0.003 ± 0.003 1950-2009	-0.002 ± 0.007 1950-1979	$+0.005 \pm 0.022$ 1990-2009
336				
337	Area F	5°S-0°N, 90°E-98°E, 50-300 m		
338	Temperature	-0.002 ± 0.028 1960-2016	$+0.004 \pm 0.056$ 1960-1990	$+0.033 \pm 0.163$ 1995-2016
339	Salinity	$+0.0020 \pm 0.0025$ 1960-2016	$+0.0049 \pm 0.0038$ 1960-1996	$+0.0043 \pm 0.0071$ 1995-2016
340	Oxygen	-0.221 ± 0.263 1960-2016	-0.098 ± 0.765 1960-1990	$+0.123 \pm 1.220$ 1995-2016
341	Nitrate	$+0.036 \pm 0.174$ 1962-2007	-0.130 ± 0.581 1962-1984	$-0.207 \pm \text{NaN}$ 1995-2007
342	Silicate	$+0.033 \pm 0.410$ 1960-2007	$+0.173 \pm 0.619$ 1960-1990	$-0.368 \pm \text{NaN}$ 1995-2007
343	Phosphate	$+0.003 \pm 0.009$ 1960-2007	$+0.003 \pm 0.014$ 1960-1989	$-0.015 \pm \text{NaN}$ 1995-2007
344				
345				
346				
347				

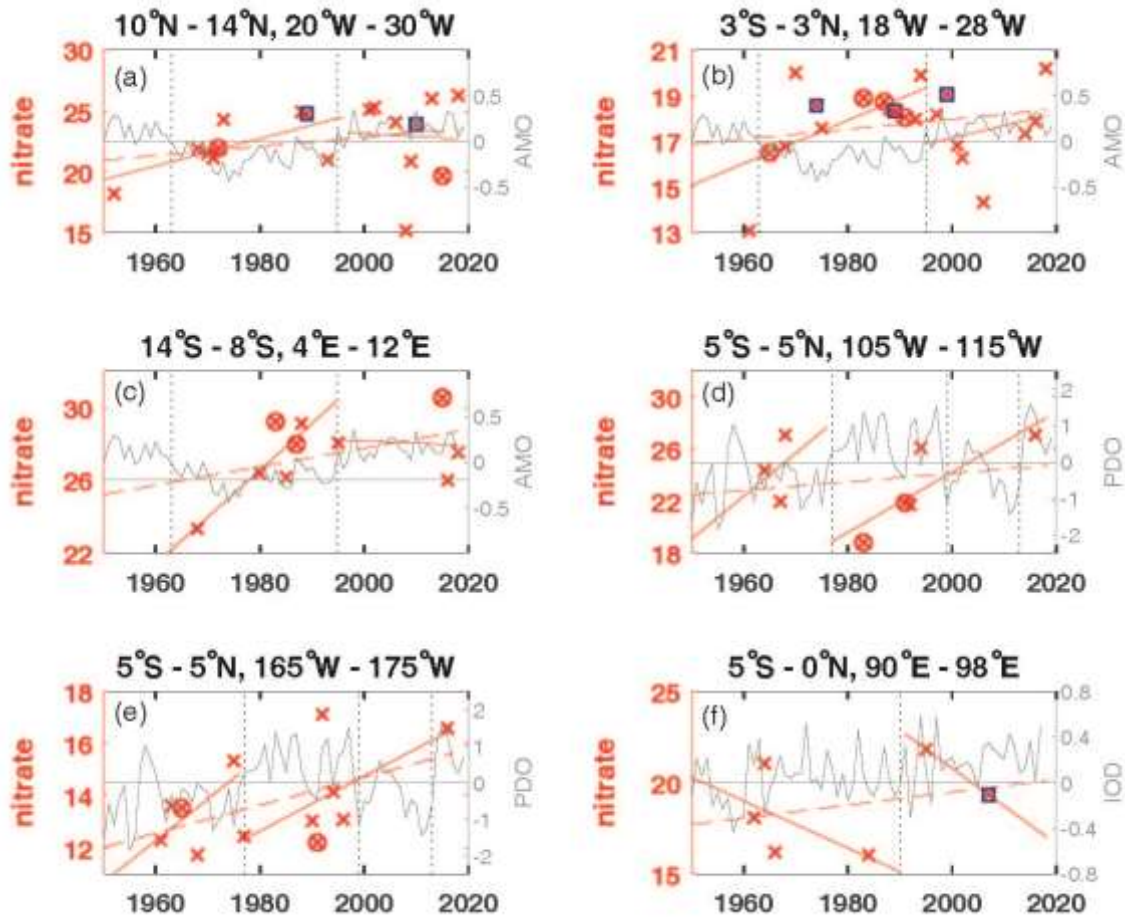
348
349
350
351



352
353

354 **Figure 3:** Annual mean oxygen concentration for years available (x) used to calculate trends for the layer 50 to 300 m in μmol
355 kg⁻¹ plotted for the available years in the time period 1950 to 2018 (dashed red line) and for the positive and negative periods
356 of the AMO in the Atlantic (a-c), the PDO in the Pacific (d,e) and the IOD in the Indian Ocean (f) as solid red lines. The AMO,
357 PDO and IOD are shown as grey lines. The change of AMO status in 1963 and 1995, the change of the PDO phase in 1977,
358 1999 and 2013 and the IOD in 1990 are marked by dotted vertical lines. El Niño years defined as strong are marked by an
359 additional magenta circle, strong La Niña years by an additional blue square. The scale of the y-axis changes according to the
360 oxygen concentration range of each area.

361
362
363
364
365
366



367
368
369

370 **Figure 4:** Annual mean nitrate concentration for years available (x) used to calculate trends for the layer 50 to 300 m in μmol
371 kg^{-1} plotted for the available years in the time period 1950 to 2018 (dashed red line) and for the positive and negative periods
372 of the AMO in the Atlantic (a-c), the PDO in the Pacific (d,e) and the IOD in the Indian Ocean (f) as solid red lines. For area
373 A the nitrate measurements in 1974 were removed as the 50-300 m mean was much too low $2.93 \mu\text{mol kg}^{-1}$ and for area D the
374 nitrate measurements were removed in 1970 which were too high ($30.28 \mu\text{mol kg}^{-1}$). The AMO, PDO and IOD are shown as

375 grey lines. The change of AMO status in 1963 and 1995, the change of the PDO phase in 1977, 1999 and 2013 and the IOD
376 in 1990 are marked by dotted vertical lines. El Niño years defined as strong are marked by an additional magenta circle, strong
377 La Niña years by an additional blue square. The scale of the y-axis changes according to the nitrate concentration range of
378 each area.

379

380

381 While oxygen decreased in all areas except for area C in the eastern tropical South Atlantic for the entire time period in the 50
382 to 300 m layer (Figure S1), nitrate increased in all areas (Figure 4; Figure S1). Phosphate also increased in the Atlantic and
383 Indian Ocean areas, while it decreased in the 2 areas of the equatorial Pacific Ocean (Table 2). Silicate decreased in the Atlantic
384 and Pacific areas but increased in the eastern Indian Ocean (area F). The temperature decreased in the central equatorial Pacific
385 and the eastern Indian Ocean (areas E and F) as is the case for these areas also in the 300 to 700 m layer. Surprisingly at the
386 equatorial area in the Atlantic (area B) the temperature in the 50 to 300 m layer decreased while it increased in the 300 to 700
387 m layer. The 50 to 300 m layer at the equator is governed by the eastward flowing Equatorial Undercurrent (EUC) while in
388 the 300 to 700 m layer the westward flowing Intermediate Undercurrent (IUC) is located which might have an influence on
389 the temperature change over time. The salinity in the 50 to 300 m layer increased in all areas except for a stagnant salinity
390 concentration in the eastern tropical Pacific Ocean (area D; Table 2).

391 The largest amount of years with available nutrient data exists in area A in the Atlantic Ocean. The long-term trends in area A
392 for temperature and oxygen for the 50 to 300 m layer (Table 2, Figure 5a,c) are similar as for the deeper layer 300 to 700 m
393 (Table 1), however with increased variability near the surface most likely influenced by the seasonal cycle. For the 3 Atlantic
394 areas A, B and C the long-term 50 to 300 m trend decreased for oxygen (except for area C) and silicate, and increased for
395 salinity, nitrate, phosphate and temperature, the latter except for temperature in area B with a weak not significant temperature
396 decrease. In the Atlantic, the equatorial station B shows higher mean 50 to 300 m layer temperature, salinity and oxygen and
397 lower mean nitrate, silicate and phosphate values compared to the off-equatorial stations A and C (Table 3) and shows the
398 eastward transport of oxygen-rich water with the EUC to the low oxygen regions in the eastern tropical Atlantic. Although the
399 oxygen trend in the 50 to 300 m layer of area B is weaker than for areas A, D, E and F the standard deviation for oxygen is
400 larger than in the other areas. This is not due to the trend but originates in the large variability from year to year (Figure 3)
401 probably related to a variable oxygen distribution across the equator between 3°N and 3°S.

402

403

404

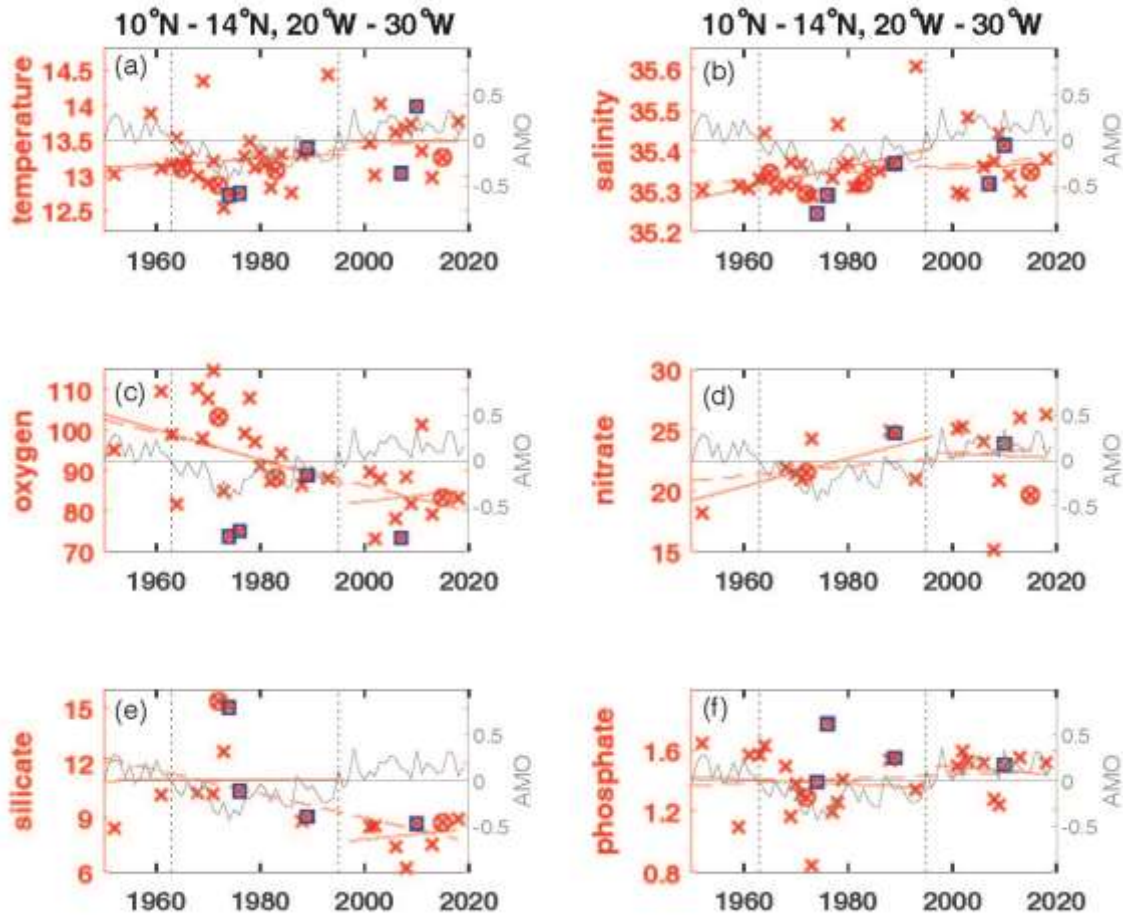
405

406

407

408

409
410
411
412
413



414
415
416

417 **Figure 5:** Annual mean parameter concentration for years available (x) used to calculate trends for the layer 50 to 300 m
418 plotted for the available years in the time period 1950 to 2018 (dashed red line) and for the positive and negative periods of
419 the AMO in the Atlantic at area A for temperature (a) in $^{\circ}\text{C}$, salinity (b), oxygen (c) in $\mu\text{mol kg}^{-1}$, nitrate (d) in $\mu\text{mol kg}^{-1}$,
420 silicate (e) in $\mu\text{mol kg}^{-1}$ and phosphate (f) in $\mu\text{mol kg}^{-1}$. The AMO is shown as a grey line. The change of AMO status in 1963
421 and 1995 is marked by dotted vertical lines. El Niño years defined as strong are marked by an additional magenta circle, strong
422 La Niña years by an additional blue square.

423

424

425 **Table 3.** Mean parameter values with number of profiles and standard deviation for the time period covered derived from the
 426 annual mean parameter value in brackets for the layers 50-300 m and 300 to 700 m of temperature in °C, salinity and solutes
 427 in $\mu\text{mol kg}^{-1}$ in the Atlantic Ocean (areas A, B, C), in the Pacific Ocean (areas D, E) and in the Indian Ocean (area F).

428

429 Parameter	area A	area B	area C	area D	area E	area F
430 50-300 m						
431 Temperature	13.24 (39;0.44)	14.96 (44;0.55)	13.38 (29;0.58)	13.91 (31;0.81)	19.29 (34;1.02)	17.00 (28;1.09)
432 Salinity	35.35 (39;0.06)	35.43 (45;0.04)	35.33(29;0.06)	34.89 (31;0.05)	35.12 (31;0.12)	35.01 (28;0.07)
433 Oxygen	91.05 (33;11.57)	109.89 (44;20.34)	55.18 (23;18.47)	70.06 (27;17.91)	141.12 (31;12.56)	96.16 (22;8.51)
434 Nitrate	22.52 (18;2.96)	17.75 (21;1.74)	27.44 (10;2.04)	23.63 (9;3.57)	13.77 (12;1.74)	18.76 (6;2.43)
435 Silicate	9.72 (18;2.38)	7.52 (26;2.03)	10.74 (11;1.68)	20.59 (7;2.30)	10.33 (11;2.84)	19.92 (15;7.84)
436 Phosphate	1.41 (28;0.20)	1.15 (35;0.15)	1.73 (13;0.13)	1.83 (9;0.18)	1.15 (15;0.20)	1.40 (16;0.20)
437						
438 300 – 700 m						
439 Temperature	9.16 (32;0.30)	7.42 (41;0.23)	7.80 (24;0.22)	8.40 (29;0.18)	8.35 (27;0.23)	9.81 (24;0.32)
440 Salinity	35.02 (32;0.05)	34.67 (41;0.03)	34.73 (25;0.04)	34.66 (29;0.01)	34.65 (26;0.02)	34.97(24;0.04)
441 Oxygen	62.19 (29;7.49)	104.49 (40;29.76)	47.25 (16;4.40)	32.99 (26;6.39)	72.03 (25;10.11)	67.92 (19;6.25)
442 Nitrate	34.46 (16;1.64)	31.28 (20;2.72)	39.28 (9;1.64)	35.66 (9;3.48)	32.97 (11;2.78)	31.44(5;2.09)
443 Silicate	17.51 (16;3.60)	19.31 (28;3.80)	22.05 (10;2.14)	43.91 (7;3.18)	38.10 (10;3.67)	38.40 (14;7.00)
444 Phosphate	2.10 (28;0.15)	2.04 (34;0.16)	2.47 (12;0.15)	2.66 (9;0.17)	2.46 (12;0.07)	2.15 (11;0.15)

445

446 In the 50 to 300 m layer of area A despite the expected generally lower oxygen during positive AMO phase oxygen increased
 447 in the positive AMO phase after 1995 (Figure 3a) different to the decrease in the 300 to 700 m layer (Figure 2a). During the
 448 positive AMO phase after 1995 in the 50 to 300 m layer of area A trends in temperature, oxygen, nitrate, silicate and phosphate
 449 (Figure 5) changed sign compared to the long-term trend while salinity showed for this period the same continuous trend as
 450 the positive long-term trend. In contrast none of these parameters changed during positive AMO compared to the long-term
 451 trend at the 50 to 300 m layer in the equatorial Atlantic in area B. In the tropical North Atlantic (area A) and the equatorial
 452 Atlantic (area B) the La Niña events showed lower than normal oxygen concentrations especially for the years 1973/74,
 453 1975/76 and 2010/11 (Figure 3a,b). These years were not covered in the eastern tropical South Atlantic (area C). In the
 454 equatorial area B, the El Niño years 1965/66, 1972/73, 1987/88 and 1991/92 showed slightly higher than normal oxygen
 455 concentrations (Figure 3b). Although not true for all ENSO events, there seems to be some influence of the La Niña and El

456 Niño events in the eastern tropical and equatorial Atlantic, which might be due to the various types with different hydrographic
457 impact of ENSO events described in literature.

458 In eastern Pacific regions near the Galapagos Islands (2-5°S, 84-87°W) and near the American continent in the CalCofi region
459 (34-35°N, 121-122°W) and the Peru region (7-12°S, 78-83°W) oxygen increased and nutrients decreased in the 50 to 300 m
460 layer during the negative PDO phase before 1977 with opposing trends during the positive PDO phase after 1977 (Stramma et
461 al. 2020). Different to the eastern Pacific the eastern and central and equatorial areas D and E (Table 2) don't show the reversed
462 trends in oxygen and nutrients, however temperature and salinity indicate a reversal with the PDO phase as the PDO index
463 encapsulates the major mode of sea surface temperature variability in the Pacific. On a global scale the long-term SST trend
464 1901-2012 was positive everywhere except for a region in the North Atlantic (IPCC 2013, Fig. 2.21). For 1981 to 2012, while
465 the western Pacific showed a warming trend, a large region with decreasing SST's was seen in the eastern and equatorial
466 Pacific Ocean (IPCC 2013, Fig. 2.22). This agrees with the temperature reversal seen in areas D and E. However, if the time
467 period after 1977 is looked at separately for the positive PDO phase 1977 to 1999 and the negative PDO phase 1999 to 2013
468 similar as in the layer 300 to 700 m also the layer 50 to 300 m shows the expected high oxygen concentrations in the period
469 1977 to 1990 and lower oxygen concentrations during 1999 to 2010 (Figure 3d,e).

470 Although ENSO is a signal originating in the Pacific the equatorial Pacific areas D and E show no obvious oxygen
471 concentration changes related to ENSO events (Figure 3d,e). The central equatorial Pacific area E shows the highest mean 50
472 to 300 m temperature and oxygen concentrations and the lowest nitrate concentrations of all six areas investigated (Table 3).
473 The low nitrate and phosphate and lower silicate compared to the eastern equatorial area D shows the nutrient concentration
474 decreasing westward in the equatorial Pacific in the 50 to 300 m layer (Stramma et al., 2020; their Figure 2). The principal
475 source of nutrients to surface water is vertical flux by diffusion and advection and by regeneration (Levitus et al., 1993). At
476 the sea surface airborne nutrient supply from land is contributed as well as terrestrial runoff of fertilizer-derived nutrients and
477 organic waste adding nutrients to the ocean (Levin, 2018). The tongue of high nutrient concentrations at the equatorial Pacific
478 compared to the subtropical Pacific results from upwelling near the American shelf (Levitus et al., 1993) and equatorial
479 upwelling.

480 In the eastern Indian Ocean as in the 300 to 700 m layer the temperature in the 50 to 300 m layer (Table 2) decreases and
481 indicates other processes related to the oxygen decrease instead of warming. In the Indian Ocean the IOD shows large
482 variability on shorter time scales. Observations indicate that positive IOD events prevent anoxia off the west coast of India
483 (Vallivattathillan et al. 2017). The IOD is very variable with a slightly higher index after 1990. The few oxygen measurements
484 in the 50 to 300 m layer indicate in area F until 1990 high mean oxygen concentrations with a decrease in oxygen and after
485 1990 low oxygen concentrations with an increase in oxygen (Figure 3f). The higher oxygen concentrations before 1990 and
486 lower oxygen concentrations afterwards are also visible in the 300 to 700 m layer (Figure 2f). The ENSO events don't indicate
487 a visible influence on the oxygen concentration in area F. The four La Niña events between 1988 and 2008 were either below
488 or above the mean trend-line; the same is true for the two El Niño events in 1973/74 and 1987/88 (Figure 3f).

489

490

491 **4 Discussion and Summary**

492 The time-series expansion of the six areas in the tropical oceans to the period 1950 to 2018 years showed a similar decrease in
493 oxygen in the 300 to 700 m layer as described for the 1960 to 2008 period. Therefore, despite the overlying variability the
494 long-term deoxygenation in the tropical oceans is continuous for the 68-year period (Fig. S1). This confirms the indicated
495 importance on the 48-year period (Stramma et al. 2008) of the oxygen trend for future oceanic scenarios. The salinity trends
496 are weak and not statistically significant, except for a salinity increase of 0.0012 yr^{-1} in the 300 to 700 m layer of area A in the
497 tropical Northeast Atlantic. A consistent pattern in vertical sections in the Pacific Ocean is that nitrate and phosphate increase
498 with depth to about 500 m, with a slight maximum at intermediate depths of 500–1500 m, while silicate continues to increase
499 with depth (Fiedler and Talley, 2006) which is well visible in the higher mean concentrations in the 300 to 700 m layer in
500 comparison to the 50 to 300 m layer (Table 3).

501 The temperature trends were positive in the three Atlantic areas, but positive or negative in relation to the time period included
502 in the Pacific and Indian Ocean areas. Hence, we can conclude that the decreasing oxygen is not fully coupled to the local
503 temperature change. As the decline of oxygen in the tropical Pacific was not accompanied by a temperature increase, Ito et al.
504 (2016) concluded that the cause of the oxygen decline must include changes in biological oxygen consumption and/or ocean
505 circulation. Modelling the depth range 260 to 710 m depth range for 1990s-1970s the region of our areas D and E were mainly
506 influenced by circulation variability (Ito et al., 2016).

507 Enhanced temperature differences between land and sea could intensify upwelling winds in eastern upwelling areas (Bakun,
508 1990). Observed and modelled changes in wind in the Atlantic and Pacific over the past 60 years appear to support the idea of
509 increased upwelling winds (Sydeman et al., 2014). Coastal and equatorial upwelling enhance nutrients in the upper ocean;
510 therefore, the increase of nutrients in the eastern and equatorial oceans might be caused by winds intensifying upwelling. More
511 nutrients in the surface layer enhances production and subsequently export and thus at greater depth its decay with increased
512 respiration reduces the oxygen content. The sinking flux of organic matter, which over time depletes oxygen, while adding
513 carbon and nutrients to subsurface waters, is known as the biological pump (Keeling et al., 2010) and could cause the often
514 observed opposite trends in oxygen and nutrient trends in the 50 to 300 m layer investigated here. In the 50 to 300 m layer
515 oxygen, temperature, salinity and nutrients showed long-term trends, which were different in the three ocean basins. Nitrate
516 increased in all areas. Phosphate also increased in the Atlantic and Indian Ocean areas, while it decreased in the two areas of
517 the equatorial Pacific Ocean. The phosphate increase in the Atlantic Ocean might be related to a continuous phosphate supply
518 with the Saharan dust distributed over the Atlantic Ocean with the wind (Gross et al. 2015). Silicate decreased in the Atlantic
519 and Pacific areas but increased in the eastern Indian Ocean. Often the expected inverse trend of oxygen and nutrients caused
520 by remineralization of marine detritus (Whitney et al. 2013) was observed; however, variations based on other drivers influence
521 the nutrient trends.

522 To summarize the results for the different Ocean basins in the Atlantic Ocean; oxygen decreases and temperature and salinity
523 increase for both depth layers except in the eastern tropical South Atlantic (area C) for the 50 to 300 m layer where oxygen

524 slightly increases in the Angola Dome region. In the Pacific and Indian Ocean oxygen decreases, however temperature and
525 salinity either increase or decrease. The trends for nutrients often are not in the 95% confidence range, but indicate in the
526 Atlantic a nitrate and phosphate increase with a silicate decrease, in the Pacific a nitrate increase and phosphate and silicate
527 decrease while in the eastern tropical Indian Ocean nitrate, silicate and phosphate increase. Nutrient variability indicates that
528 their trends are more dependent on local drivers in addition to a global trend.

529 An influence of ENSO years on the oxygen distribution with lower mean oxygen concentrations in the 50 to 300 m layer in
530 La Niña years and larger oxygen concentrations in El Niño years was visible in the tropical North Atlantic and equatorial
531 Atlantic. No clear impact of ENSO was observed in the tropical South Atlantic and the Pacific and Indian Ocean areas (C to
532 F).

533 To construct time series in areas with low data availability measurements from larger areas had to be taken into account. As a
534 result, there is a possible bias due to the distribution of the measurements within the area and due to gaps in the time line. In
535 addition, there might be variations due to the measurement techniques for oxygen and nutrients and the use of different
536 reference material used for nutrient measurements or applied bias for nutrient measurements. Utilization of historical nutrient
537 data to assess decadal trends has been hindered by their inaccuracy, manifested as offsets in deep water concentrations
538 measured by different laboratories (Zhang et al., 2000). Although the trends are often not 95% significant the results indicate
539 existing trends and climate related changes. As a consequence, there is the possibility of a larger variability in the computed
540 trends compared to the earlier investigation of these areas in Stramma et al. (2008). Later measurements reported in the
541 literature confirmed the described decrease in oxygen (Stramma et al. 2008) in the tropical oceans (e.g. Hahn et al. 2017). The
542 not statistical significant trends described here might be verified with additional data in the future, especially in case the drift
543 observed in float measurements can be removed and float data be added to extend the data sets. Changing the depth layer of
544 the trend computations leads to different mean parameter values (Table 3) and may result in some minor variations in the trend
545 computation. However, as the oxygen trends for the 50 to 300 m layer and the 300 to 700 m are all negative (except for the 50
546 to 300 m layer of area C due to a local effect) the result of oxygen decrease is not related to the depth layer chosen.

547
548 Although the data base is small especially for nutrients there is an indication that variability overlain on the long-term trends
549 is connected to climate modes as was found in the eastern Pacific with reversing trends related to the PDO (Stramma et al.,
550 2020). The six areas of the tropical ocean basins indicate some connection to the climate modes of the 3 ocean basins. In the
551 tropical eastern North Atlantic (area A) there is some dependence with the AMO. In the equatorial Pacific areas D and E a
552 connection to the PDO is visible when the positive PDO phase 1977 to 1999 and the negative PDO phase 1999 to 2013 are
553 looked at separately. In the eastern tropical Indian Ocean there seems to be some dependence to the state of the IOD, despite
554 the fact that the IOD varies more on shorter time scales and the IOD change in 1990 is weak.

555 Future measurements of temperature, salinity, oxygen and nutrients could lead to more stable results determining trends and
556 their variability to better understand the influence of climate change on the ocean ecosystem and prepare future predictions of
557 ocean oxygen from Earth System Models (Frölicher et al., 2016). Making existing nutrient data public which are so far not in

558 public data bases and modelling efforts on oxygen and nutrient changes would further improve the understanding of oxygen
559 and nutrient variability and its biological influence e.g. on fisheries. First ecosystem changes like habitat compression can be
560 observed and negative impacts are expected on biological regulation, nutrient cycling and fertility, and sea food availability
561 with an increasing risk of fundamental and irreversible ecological transformations (Hoegh-Guldberg and Bruno, 2010). The
562 implication of oxygen trends for biology and successively human impacts is quite large and a lot of literature supports this. All
563 aspects of oxygen trends are discussed in the different chapters of the IUCN report (Laffoley and Baxter, 2019)).

564

565

566

567 *Data availability.* The AMO time series was taken from <https://www.esrl.noaa.gov/psd/data/timeseries/AMO/> (ESRL, Climate
568 time series, status 17.02.2020). The Indian Ocean Dipole Mode was taken from
569 https://www.esrl.noaa.gov/psd/gcos_wgsp/Timeseries/Data/dmi.long.data on 3 March 2020. The yearly PDO data were taken
570 from http://ds.data.jma.go.jp/tcc/tcc/products/el_nino/decadal/annpdo.txt on 9 July 2020 from the Japan Meteorological Society
571 covering the period 1901 to 2019.

572 The bottle data from cruises in 2016 at 170°W (096U2016426_hyd1.csv) and at 110°W (33RO20161119_hyd1.csv) were
573 downloaded from the CCHDO at the University of California San Diego (<https://cchdo.ucsd.edu>, CCHDO, 2020) on 8
574 November 2018.

575 The added ship cruises are contained for CTD data in the data sets for RV Meteor cruise M119
576 <https://cloud.geomar.de/s/tmJWCFJ27gPBmpa>, for RV Meteor cruises M120
577 <https://doi.pangaea.de/10.1594/PANGAEA.868654> (Kopte and Dengler 2016), M130
578 <https://doi.pangaea.de/10.1594/PANGAEA.903913> (Burmeister et al. 2019), M131
579 <https://doi.pangaea.de/10.1594/PANGAEA.910994> (Brandt et al. 2020), M145
580 <https://doi.pangaea.de/10.1594/PANGAEA.904382> (Brandt and Krahnmann, 2019), and, for RV Meteor cruise M148
581 <https://cloud.geomar.de/s/tmJWCFJ27gPBmpa>, and RV Merian 07 <https://cloud.geomar.de/s/tmJWCFJ27gPBmpa>
582 and for nutrient data in the data sets of Merian MSM10/1 <https://doi.pangaea.de/10.1594/PANGAEA.775074> (Tanhua et al.
583 2012), RV Poseidon 250 <https://cloud.geomar.de/s/tmJWCFJ27gPBmpa>, M68/2
584 <https://www.ncei.noaa.gov/data/oceans/nci/ocads/data/0108078/>, M83/1 <https://doi.pangaea.de/10.1594/PANGAEA.821729>
585 (Tanhua 2013). M97 <https://doi.pangaea.de/10.1594/PANGAEA.863119> (Tanhua 2016), Meteor M106
586 <https://cloud.geomar.de/s/tmJWCFJ27gPBmpa>, Meteor M119 <https://cloud.geomar.de/s/tmJWCFJ27gPBmpa>,
587 <https://cloud.geomar.de/s/tmJWCFJ27gPBmpa>, Meteor M130 <https://doi.pangaea.de/10.1594/PANGAEA.913986> (Tanhua
588 2020), Meteor M131 <https://cloud.geomar.de/s/tmJWCFJ27gPBmpa>, Meteor M145
589 <https://cloud.geomar.de/s/tmJWCFJ27gPBmpa>, and Meteor M148 <https://cloud.geomar.de/s/tmJWCFJ27gPBmpa>.

590

591 *Author contributions.* L. Stramma conceived the study and wrote the manuscript. S. Schmidtke compiled the data for the time
592 series, collected further references and discussed and modified the manuscript.

593

594 *Competing interests.* The authors declare that they have no conflict of interest.

595 .

596 *Acknowledgements.* Financial support was received through GEOMAR and the Deutsche Forschungsgemeinschaft (DFG) as
597 part of the “Sonderforschungsbereich 754: Climate-Biogeochemistry Interactions in the Tropical Ocean”.

598 **References**

599 Allison, E.H., and Bassett, H.R.: Climate change in the oceans: Human impacts and responses, *Science*,
600 350, 778-782. <https://doi.org/10.1126/science.aac8721>, 2015.

601 Ayers, J. M., Strutton, P. G., Coles, V. J., Hood, R. R., and Matear, R. J.: Indonesian throughflow
602 nutrient fluxes and their potential impact on Indian Ocean productivity, *Geophysical Research*
603 *Letters*, 41, 5060–5067, doi:10.1002/2014GL060593, 2014.

604 Bakun A.: Global climate change and the intensification of coastal upwelling, *Science* 247,198–201,
605 1990.

606 Bastin, S., Claus, M., Brandt, P., and Greatbatch, R. J.: Equatorial deep jets and their influence on the
607 mean equatorial circulation in an idealized ocean model forced by intraseasonal momentum flux
608 convergence, *Geophysical Research Letters*, 47, e2020GL087808.
609 <https://doi.org/10.1029/2020GL087808>, 2020.

610 Bograd, S. J., Pozo Buil, M., Di Lorenzo, E., Castro, C. G., Schroeder, I. D., Goericke, R., Anderson, C.
611 R., Benitez-Nelson, C., and Whitney, F. A.: Changes in source waters to the Southern California
612 Bight, *Deep-Sea Res. II*, 112, 42-52, <https://doi.org/10.1016/j.dsr2.2014.04.009>, 2015.

613 Brandt, P., and Krahnmann, G.: Physical Oceanography (CTD) during METEOR cruise M145,
614 PANGAEA, <https://doi.org/101594/PANGAEA.904382>, 2019.

615 Brandt, P., Kopte, R., and Krahnmann, G.: Physical oceanography (CTD) during METEOR cruise M131.
616 PANGAEA, <https://doi.org/10.1594/PANGAEA.910994>, 2020.

617 Bretherton, F. P., Davis, R. E., and Fandry, C. B.: A technique for objective analysis and design of
618 oceanographic experiments applied to MODE-73, *Deep-Sea Research*, 23, 559-582,
619 [https://doi.org/10.1016/0011-7471\(76\)90001-2](https://doi.org/10.1016/0011-7471(76)90001-2), 1976.

620 Burmeister, K., Lübbecke, J., Brandt, P., Claus, M., and Hahn, J.: Ventilation of the eastern tropical
621 North Atlantic by intraseasonal flow events of the North Equatorial Undercurrent. PANGAEA,
622 <https://doi.org/10.1594/PANGAEA.903913>, 2019.

623 CCHDO: Welcome to the CCHDO, available at: <https://cchdo.ucsd.edu>, last access: 13 February 2020.

- 624 Cheung, W. W. L., Sarmiento, J. L., Dunne, J., Frölicher, T. L., Lam, V. W. Y., Palomares, M. L. D.,
625 Watson, R., and Pauly, D.: Shrinking of fishes exacerbates impacts of global ocean changes of
626 marine ecosystems, *Nature Climate Change*, 3, 254-258, <https://doi.org/10.1038/nclimate1691>,
627 2013.
- 628 Deser, C., Alexander, M. A., Xie, S.-P., and Phillips, A. S.: Sea surface temperature variability: Patterns
629 and mechanisms, *Annual Review of Marine Science*, 2, <https://doi.org/10.1146/annurev-marine-120408-151453>, 2010.
- 631 Deutsch, C., Brix, H., Ito, T., Frenzel, H., and Thompson, L.: Climate-forced variability of ocean
632 hypoxia, *Science*, 333, 336-339, <https://doi.org/10.1126/science.1202422>, 2011.
- 633 Fiedler, P. C., and Talley, L. D.: Hydrography of the eastern tropical Pacific: A review, *Progress in*
634 *Oceanography*, 69, 143-180, 2006.
- 635 Frölicher, T. L., Rogers, K. B., Stock, C. A., and Cheung, W. L. W.: Sources of uncertainties in 21th
636 century projections of potential ecosystem stressors, *Global Biological Cycles*, 30, 1224-1243,
637 <https://doi.org/10.1002/2015GB005338>, 2016.
- 638 Gilly, W. F., Beman, J. M., Litvin, S. Y., and Robinson, B. H.: Oceanographic and biological effects of
639 shoaling of the oxygen minimum zone, *Annual Review of Marine Science*, 5,
640 <https://doi.org/10.1146/annurev-marine-120710-100849>, 2013.
- 641 Gouretski, V. V., and Jancke, K.: Systematic errors as the cause for an apparent deep water property
642 variability: Global analysis of the WOCE and historical hydrographic data, *Progress in*
643 *Oceanography*, 48, 337-402, 2001.
- 644 Gross, A., Goren, T., Pio, C, Cardoso, J., Tirosh, O., Todd, M.C., Rosenfeld, D., Weiner, T., Custódio,
645 D., and Angert, A.: Variability in Sources and Concentrations of Saharan Dust Phosphorus over
646 the Atlantic Ocean, *Environmental Science & Technology Letters*, 2, 2, 31–37, 2015.
- 647 Hahn, J., Brandt, P., Schmidtko, S., and Krahnemann, G.: Decadal oxygen change in the eastern tropical
648 North Atlantic, *Ocean Sci.*, 13, 551-576, <https://doi.org/10.5194/os-13-551-2017>, 2017.
- 649 Ham, Y., Choi, J., and Kug, J.: The weakening of the ENSO–Indian Ocean Dipole (IOD) coupling
650 strength in recent decades, *Climate Dynamics*, 49, 249–261, <https://doi.org/10.1007/s00382-016-3339-5>, 2017.
- 652 Hoegh-Guldberg, O., and Bruno, J. F.: The impact of climate change on the world’s marine ecosystems,
653 *Science*, 328, 1523-1528.
- 654 Hurrell, J. W., and Deser, C.: North Atlantic climate variability: The role of the North Atlantic Oscillation,
655 *Journal of Marine Systems*, 79, 231-244, <https://doi.org/10.1016/j.jmarsys.2009.11.002>, 2010.
- 656 IPCC: Climate Change 2013: The Physical Science Basis. Contribution of Working Group I to the Fifth
657 Assessment Report of the Intergovernmental Panel on Climate Change. Stocker, T. F., Qin, D.,
658 Plattner, G.-K., Tignor, M., Allen, S. K., Boschung, J., Nauels, A., Xia, Y, Bex, V., and Midgley,
659 P. M. (eds.). Cambridge University Press, Cambridge, United Kingdom and New York, NY, USA,
660 1535 pp, 2013.

661 Ito, T., Nenes, A., Johnson, M. S., Meskhidze, N., and Deutsch, C.: Acceleration of oxygen decline in the
662 tropical Pacific over the past decades by aerosol pollutants, *Nature Geoscience*, 9, 443-448,
663 <https://doi.org/10.1038/NGEO2717>, 2016.

664 Ito, T., Minobe, S., Long, M. C., and Deutsch, C.: Upper ocean O₂ trends: 1958-2015, *Geophysical
665 Research Letters*, 44, 4214-4223, doi:10.1002/2017GL073613, 2017.

666 Johnson, G.C., Robbins, P.E., and Hufford, G.E.: Systematic adjustments of hydrographic sections for
667 internal consistency. *J. Atmos. Ocean. Technol.*, 18(7), 1234–1244, doi: 10.1175/1520-
668 0426(2001)018<1234:SAOHSF>2.0.CO;2, 2001.

669 Keeling, R. F., Körtzinger, A., and Gruber, N.: Ocean deoxygenation in a warming world, *Annual Review
670 of Marine Science*, 2, 199-229, 2010.

671 Kopte, R., and Dengler, M.: Physical oceanography during METEOR cruise M120. PANGAEA,
672 <https://doi.org/10.1594/PANGAEA.868654>, 2016.

673 Laffoley, D., and Baxter, J. M. (eds): Ocean deoxygenation: Everyone’s problem – Causes, impacts,
674 consequences and solutions. Full report, Gland, Switzerland: IUCN, 580pp,
675 <https://doi.org/10.2305/IUCN.ch.2019.13.en>, 2019.

676 Latif, M., and Grötzner, A.: The equatorial Atlantic oscillation and its response to ENSO, *Climate
677 Dynamics*, 16, 213–218, <https://doi.org/10.1007/s003820050014>, 2000.

678 Levin, L. A.: Manifestation, drivers, and emergence of open ocean deoxygenation, *Annual Review of
679 Marine Science*, 10, 229-260, <https://doi.org/10.1146/annurev-marine-12916-063359>, 2018.

680 Levitus, S., Conkright, M. E., Reid, J. L., Najjar, R. G., and Mantyla, A.: Distribution of nitrate, phosphate
681 and silicate in the world oceans, *Progress in Oceanography*, 31, 254-273, 1993.

682 Li, G., Cheng, L., Zhu, J., Trenberth, K.E., Mann, M. E., and Abraham, J. P.: Increasing ocean
683 stratification over the past half-century, *Nature Climate Change*, Online: DOI:10.1038/s41558-
684 020-00918-2, 2020.

685 Louanchi, F., and Najjar, R.G.: A global monthly climatology of phosphate, nitrate, and silicate in the
686 upper ocean: Spring-summer export production and shallow remineralization, *Global
687 Biogeochemical Cycles*, 14, 957-977, 2000.

688 Mazeika, P. A.: Thermal domes in the eastern tropical Atlantic Ocean, *Limnology and Oceanography*,
689 12, 537–539, 1967.

690 McPhaden, M. J., Zebiak, S. E., and Glantz, M. H.: ENSO as an Integrating Concept in Earth Science,
691 *Science*, 314, 1740-1745, <https://doi.org/10.1126/science.1132588>, 2006.

692 Montes, E., Muller-Karger, F. E., Cianca, A., Lomas, M. W., and Habtes, S.: Decadal variability in the
693 oxygen inventory of North Atlantic subtropical underwater captured by sustained, long-term
694 oceanographic time series, *Global Biogeochemical Cycles*, 30, 460-476,
695 doi:10.1002/2015GB005183, 2016.

- 696 Nicholson, S. E.: An analysis of the ENSO signal in the tropical Atlantic and western Indian Oceans,
697 International Journal of Climatology, 17, 345-375, [https://doi.org/10.1002/\(SICI\)1097-0088\(19970330\)17:4%3C345::AID-JOC127%3E3.0.CO;2-3](https://doi.org/10.1002/(SICI)1097-0088(19970330)17:4%3C345::AID-JOC127%3E3.0.CO;2-3), 1997.
- 699 Ono, T., Shiimoto, A., and Saino, T.: Recent decrease of summer nutrients concentrations and future
700 possible shrinkage of the subarctic North Pacific high-nutrient low-chlorophyll region, Global
701 Biogeochemical Cycles, 22, GB3027, <https://doi.org/10.1029/2007GB003092>, 2008.
- 702 Oschlies, A.: NAO-induced long-term changes in nutrient supply to the surface waters of the North
703 Atlantic, Geophysical Research Letters, 28, <https://doi.org/10.1029/2000GL012328>, 2001.
- 704 Palter, J.B., Lozier, M. S., and Barber, R. T.: The effect of advection on the nutrient reservoir in the
705 North Atlantic subtropical gyre, Nature, 437, 687–692, 2005.
- 706 Saji, N. N., Goswami, B. N., Vinayachandran, P. N., and Yamagata, T.: A dipole mode in the tropical
707 Indian Ocean, Nature, 401, 360-363, <https://doi.org/10.1038/43854>, 1999.
- 708 Schmidtko, S., Johnson, G. C., and Lyman, J. M.: MIMOC: A global monthly isopycnal upper-ocean
709 climatology with mixed layers, J. Geophys. Res. Oceans, 118, 1658-1672,
710 <https://doi.org/10.1002/jgrc.20122>, 2013.
- 711 Schmidtko, S., Stramma, L., and Visbeck, M.: Decline in global oceanic oxygen content during the past
712 five decades, Nature, 542, 335-339, doi:10.1038/nature21399, 2017.
- 713 Shepherd, J.G., Brewer, P.G., Oschlies, A., and Watson, A.J.: Ocean ventilation and deoxygenation in a
714 warming world: introduction and overview, Philosophical Transactions of the Royal Society A:
715 Mathematical, Physical and Engineering Sciences, 375, 20170240.
716 <https://doi.org/10.1098/rsta.2017.0240>, 2017.
- 717 Sigman, D. M., and Hain, M. P.: The biological productivity of the ocean, Nature Education, 3 (6), 1-
718 16,2012.
- 719 Stramma, L., Johnson, G. C., Sprintall, J., and Mohrholz, V.: Expanding Oxygen-Minimum Zones in the
720 Tropical Oceans, Science, 320, 655-658, doi:10.1126/science.1153847, 2008.
- 721 Stramma, L., Prince, E. D., Schmidtko, S., Luo, J., Hoolihan, J. P., Visbeck, M., Wallace, D. W. R., Brandt,
722 P., and Körtzinger, A.: Expansion of oxygen minimum zones may reduce available habitat for
723 tropical pelagic fishes, Nature Climate Change, 2, 33-37, <https://doi.org/10.1038/nclimate1304>,
724 2012.
- 725 Stramma, L., Schmidtko, S., Bograd, S. J., Ono, T., Ross, T., Sasano, D., and Whitney, F.: Trends and
726 decadal oscillations of oxygen and nutrients at 50 to 300 m depth in the equatorial and North
727 Pacific, Biogeosciences, 17, 813-831, <https://doi.org/10.5194/bg-17-813-2020>, 2020.
- 728 Sydeman, W. J., García-Reyes, M., Schoeman, D. S., Rykaczewski, R., R., Thompson, S., A., Black, B.
729 A., & Bograd, S. J.: Climate change and wind intensification in coastal upwelling ecosystems,
730 Science, 345, 77–80, 2014.
- 731 Tanhua, T.: Hydrochemistry of water samples during METEOR cruise M83/1. PANGAEA,
732 <https://doi.org/10.1594/PANGAEA.821729>, 2013.

- 733 Tanhua, T.: Hydrochemistry of water samples during METEOR cruise M97. PANGAEA,
734 <https://doi.org/10.1594/PANGAEA.863119>, 2016.
- 735 Tanhua, T.: Hydrochemistry of METEOR cruise M130. PANGAEA,
736 <https://doi.pangaea.de/10.1594/PANGAEA.913986> (dataset in review), 2020.
- 737 Tanhua, T., van Heuven, S., Key, R. M., Velo, A., Olsen, A., and Schirnick, C.: Quality control procedures
738 and methods of the CARINA database, *Earth Syst. Sci. Data*, 2, 35-49, 2010.
- 739 Tanhua, T., Stramma, L., Desai, F., and Löscher, C. R.: Hydrochemistry and molecular biology during
740 Maria S. Merian cruise MSM10/1. IFM-GEOMAR Leibniz-Institute of Marine Sciences, Kiel
741 University, PANGAEA, <https://doi.org/10.1594/PANGAEA.775074>, 2012.
- 742 Vallivattathillam, P., Iyyappan, S., Lengaigne, M., Ethé, C., Vialard, J., Levy, M., Suresh, N., Aumont,
743 O., Resplandy, L., Naik, H., & Naqvi, W.: Positive Indian Ocean Dipole events prevent anoxia
744 off the west coast of India, *Biogeosciences*, 14, 1541-1559, [https://doi.org/10.5194/bg-14-1541-](https://doi.org/10.5194/bg-14-1541-2017)
745 [2017](https://doi.org/10.5194/bg-14-1541-2017), 2017.
- 746 Whitney, F. A., Bograd, S. J., and Ono, T.: Nutrient enrichment of the subarctic Pacific Ocean pycnocline,
747 *Geophys. Res. Lett.*, 40, 2200-2205, <https://doi.org/10.1002/grl.50439>, 2013.
- 748 Williams, R. G., and Follows, M. J.: Physical transport of nutrients and the maintenance of biological
749 production. In: Fasham, M. J. R. (eds) *Ocean Biogeochemistry. Global Change – The IGBP Series*
750 (closed), Springer, Berlin, Heidelberg, 2003.
- 751 Wishner, K. F., Outram, D. M., Seibel, B. A., Daly, K. L., and Williams, R. L.: Zooplankton in the eastern
752 tropical North Pacific: Boundary effects of oxygen minimum zone expansion, *Deep-Sea Research*
753 *Part I: Oceanographic Research Papers*, 79, 122-140, <https://doi.org/10.1016/j.dsr.2013.05.012>,
754 2013.
- 755 Zhang, J.-Z., Mordy, C. W., Gordon, L. I., Ross, A. and Garcia, H. E.: Temporal trends in deep ocean
756 Redfield ratios, *Science*, 289, 1839, <https://doi.org/10.1126/science.289.5486.1839a>, 2000.